Degradation of organic dyes by Peroxymonosulfate activated with Zn/Co-ZIF

Nguyen Trung Dung[1*], Nguyen Phuong Thao[1], Hoang Thu Huong[2], Le Hai Dang[2], Nguyen Lan Thanh[3,4]

[1] Faculty of Physics and Chemical Engineering, Le Quy Don Technical University, 236 Hoang Quoc Viet St., Bac Tu Liem District, Hanoi, Vietnam
[2] Faculty of chemistry, Hanoi National University of Education, 136 Xuan Thuy St., Cau Giay District, Hanoi, Vietnam
[3] Faculty of Environment and Natural Resources, Ho Chi Minh City University of Technology (HCMUT), 268 Ly Thuong Kiet Street, District 10, Ho Chi Minh City, Vietnam
[4] Vietnam National University Ho Chi Minh City, Linh Trung Ward, Thu Duc City, Ho Chi Minh City, Vietnam
*Email: ntdung@lqdtu.edu.vn

ARTICLE INFO

ABSTRACT

In this study, we successfully synthesized a bimetallic metal-organic framework material Zn/Co-ZIF to start Peroxymonosulfate (PMS) for organic dye degradation in the water body. Material characterization was evaluated by advanced methods, such as XRD, FT-IR, SEM, EDX, and BET. The influence of different factors on methylene blue (MB) decomposition rate was investigated. The results show that Zn/Co-ZIF has a porous structure, a high specific surface area and decomposes 98.22% MB (20 mg/L) in 4 minutes under reaction conditions of 40 mg/L catalyst, 0.814mM PMS, pH = 7. The decomposition efficiency of dyes increases in the order CR (79.85%) <RhB (90.81 %) < DB71 (96.07%) < MO (97.63%) < MB (98.22%). The main ROS for the degradation MB in this study were $SO_4^{\bullet-}$, $O_2^{\bullet-}$ and $^1O_2$. This shows that Zn/Co-ZIF materials are potential heterogeneous catalysts to activate PMS to decompose organic pollutants in water.

Introduction

The advanced oxidation process (AOP), based on Peroxymonosulfate activation (PMS), has attracted great attention from the research community. The catalytic activation of PMS in transition metal ions can create radical paths such as superoxide radical ($O_2^{\bullet-}$), sulfate radical ($SO_4^{\bullet-}$), hydroxyl radical (•OH), and non-radical path singlet oxygen ($^1O_2$). These reactive oxygen species form in situ and have strong oxidizing properties (redox potential 2.0–3.1V), capable of effectively decomposing many different organic pollutants into small toxic molecules lower or mineralized to CO_2 and H_2O. Among transition metal ions, Co^{2+} proves to be the most effective for PMS activation due to its high redox potential (Co^{3+}/Co^{2+}, 1.82 V) [1,2].

Zeolitic imidazolate framework (ZIF), which has two typical ones such as ZIF - 8, and ZIF - 67 is a branch of MOFs formed by transition metal ions (Zn^{2+}, Co^{2+}) and the organic ligand 2-methylimidazole via nitrogen atoms. ZIF not only has a manifold topology, high surface area, and porosity but also exhibits excellent thermal and chemical stability. In addition, Zn/Co-ZIF can be rapidly synthesized at ambient conditions without hydrothermal synthesis (technically difficult, costly, and less safe) or toxic solvents pretreatment [3,4]. ZIFs are widely used in adsorbents, catalysts, supercapacitors, and drug delivery. In particular, ZIF is

applied in activating PMS to treat persistent organic pollutants such as Tylosin[3], carbamazepine[4], Rhodamine B[5,6], ciprofloxacin[7]. According to the research of Teheri et al., the introduction of Zn into the Co-ZIF structure promote the resistance to water-induced degradation [8]. The Zn:Co ratio of 0.5:0.5 exhibited the best combination of crystallinity and hydro stability [9]. Research of Jiajin et al., show that CZIF-867 (ratio Zn:Co 1:1) have the highest surface area (398.7 m^2/g) and maximum adsorption followed by Langmuir equation (119.9 mg/g) compared to ZIF67 and ZIF8 [10].

In this study, Zn/Co-ZIF were synthesized by a simple solvothermal method at room temperature and used as heterogeneous catalysts to activate PMS. Methylene blue (MB) was selected as the target pollutant to evaluate the catalytic activity through PMS activation. The effects of catalyst dosage and PMS concentration, initial solution pH, MB concentration, and other dyes were studied in detail. Reactive oxygen species formed in the Zn/Co-ZIF/PMS system were identified by the quenching method, thereby helping to propose the PMS activation mechanism.

2. Experimental

2.1. Chemicals and reagents

The chemicals used for experiments were all analytical purity (99% purity) and were used directly without purification. The chemicals include $Zn(NO_3)_2.6H_2O$, $Co(NO_3)_2.6H_2O$, 2-methyl imidazole (2-MID), PMS ($KHSO_5 \cdot 0.5KHSO_4 \cdot 0.5K_2SO_4$), methylene blue (MB), rhodamine B (RhB), directly blue 71 (DB 71), congo red (CR), methyl orange (MO), methanol (MeOH), ethanol (EtOH), tert-butanol (TBA), para-benzoquinone (p-BQ), and furfuryl alcohol (FFA) were purchased from Sigma Aldrich (USA).

2.2. Preparation of Zn/Co-ZIF

Zn/Co-ZIF materials are synthesized through the following steps (Fig 1):

Step 1: Dissolve 0.582 g of Co $(NO_3)_2.6H_2O$ (2 mmol) and 0.594 g of Zn $(NO_3)2.6H_2O$ (2 mmol) into 25 mL of methanol to get solution A.

Step 2: Dissolve 2.624 g of 2-methylimidazole (32 mmol) into 30 mL of methanol to get solution B.

Step 3: Slowly add B to A, stir well for 30 minutes to obtain a light purple solution, then leave it at room temperature for 24 hours to obtain a purple precipitate.

Step 4: Remove solvent and centrifuge at 3000 rpm for 3-5 minutes. Wash the precipitate three times with alcohol and dry at 80 °C for 12 hours to obtain purple Zn/Co-ZIF

2.3. Characterization

The morphology of the material was performed with SEM (JEOL JSM – IT 800) at acceleration voltage 30 kV. The phase composition of the Zn/Co-ZIF crystal was measured by XRD (Bruker D8 Advance) with a scanning speed of 0.01 deg/s and a 2θ range from 5° to 70° using an X-ray diffractometer Ultima IV at 40 kV/40 mA with Cu K radiation (λ= 1.5418 A°). Fourier transform infrared spectroscopy (ATR–FTIR, Perkin Elmer) with a scanning range from 4000 cm^{-1} to 400 cm^{-1} was used to detect the functional groups of the sample. The surface area results of the catalyst were obtained by Brunauer-Emmett-Teller (BET) using a TriStar II Plus 2.03 analyser at 77 K.

2.4. Degradation of organic dyes

The decomposition of organic pollutants such as MB, RhB, MO, DB71 and CR was used to evaluate the oxidation capacity of the Zn/Co-ZIF /PMS system.

The MB decomposition experiment was performed in a 250-mL glass beaker and maintained at a temperature of 25 °C. Take 100 mL of MB at 20 mg/L, add 40 mg/L of catalyst, and sonicate for 5 minutes to disperse the material. The suspension is stirred for the first 30 minutes to achieve adsorption-desorption equilibrium. Next, add 0.814 mM PMS to start the pollutant decomposition reaction. The solution pH was maintained at 7 with 0.1 M NaOH and 0.1 M H_2SO_4 solution. Next, 4 mL of water samples were filtered through membrane (0.22 μm) and analyzed by a UV–Vis device at λ = 665 nm(SP60, Biochrome, UK). The experiments were repeated twice to obtain the mean value and standard deviation. The influence of factors such as MB content (10–25 mg/L), catalyst (0–80 mg/L), PMS (0–750 mg/L), and initial pH (3.5–11) has been investigated in detail. Other pollutants such as DB 71 (λ_{max} = 586 nm), RhB (λ_{max} = 554 nm), CR (λ_{max}= 498 nm), and MO (λ_{max} = 464 nm) were measured under the same conditions as MB. Identification of reactive oxygen species such as •OH, $SO_4^{\bullet-}$, $O_2^{\bullet-}$, and $^1O_2$ was carried out by quenching experiments using different radical catchers such as TBA (500 mM), p-BQ (1 mM), EtOH (500 mM), and FFA (10 mM), respectively. MB decomposition efficiency is determined through expressions (1) [11].

$$H\ (\%) = (1 - \frac{A_t}{A_o}).100 \quad (1)$$

Here C_o and A_o, C_t and A_t are the MB optical absorption and content at the initial time, and t and k are the pseudo-first-order decay rate constants.
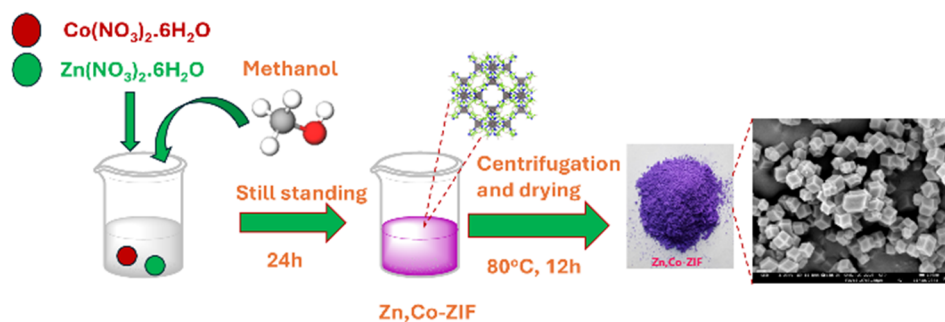
Fig 1: Synthesis of Zn/Co-ZIF catalyst
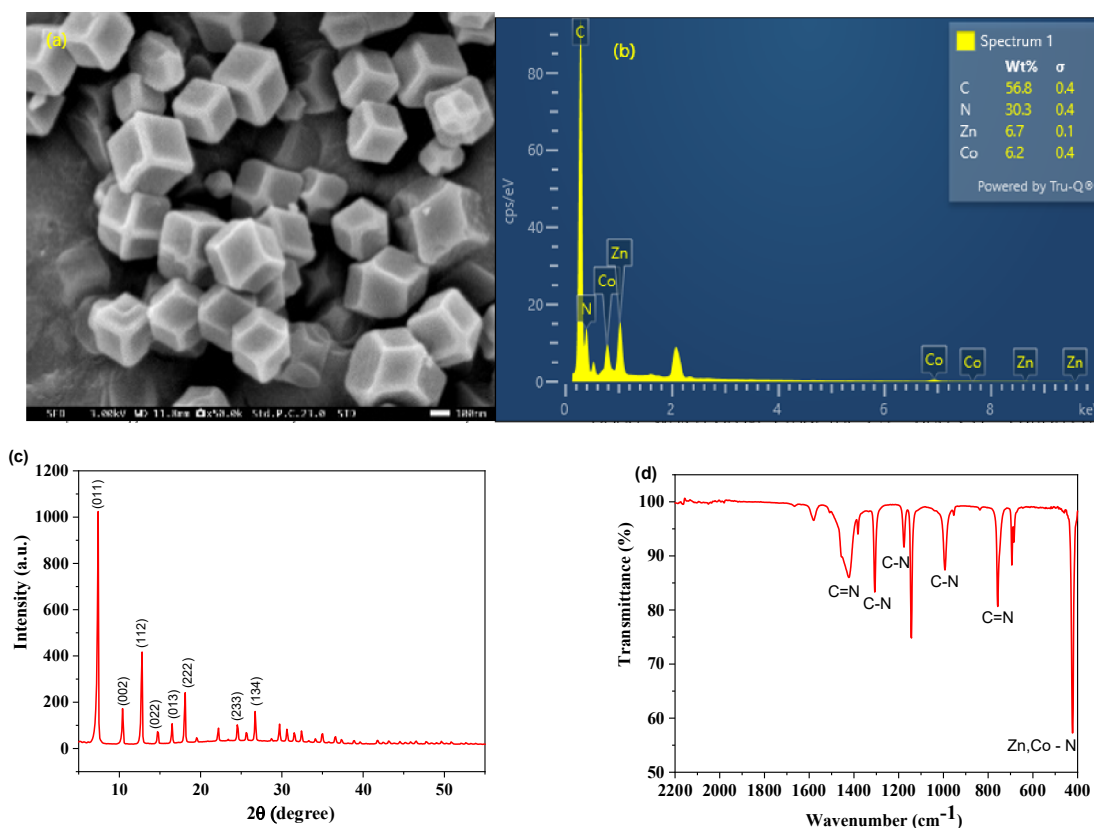
Figure 2: (a). SEM images, (b) EDS spectrum, (c) XRD pattern and (d) FT-IR spectra of Zn/Co-ZIF catalyst.

3. Results and discussion

3.1. Characterization of Zn/Co-ZIF

Zn/Co-ZIF was formed by complexing Zn^{2+} and Co^{2+} with the ligand 2-MID. The Zn/Co-ZIF crystal morphology is shown in Figure 2a. SEM images show that the Zn/Co – ZIF materials displayed a regular rhombic dodecahedron with a smooth surface (~200nm) [12]. This proved that Zn and Co precipitated simultaneously but the structure of ZIF was not broken. The EDX spectrum (Figure 2b) also demonstrates that Zn, Co, and ZIF contain the elements Zn, Co, N, and C. The ratio Zn:Co = 6.7:6.2 ≈ 1:1 is consistent with the number of moles of Zn and Co elements used in synthesis. X-ray diffraction spectra show that Zn/Co-ZIF

has a zeolite-like structure with high crystallinity, typically at peaks of 2θ=7.31; 10.49; 12.73; 14.59; 16.51; 18.21; 24.58 and 26.75 corresponds to the planes (011), (002), (112), (022), (013), (222), (233) and (134) [4,13]. (Figure 2c). Thus, from the XRD spectra, EDX successfully synthesized Zn, Co, and ZIF by the precipitation method under normal conditions.

FTIR spectroscopy (Figure 2d) determined the surface functional groups of the synthesized products. The Zn/Co-ZIF material has absorption peaks at 752 cm^{-1} and 1580 cm^{-1} because of out-of-plane vibrations and stretching vibrations of the C=N bond in the imidazole ring. In addition, the peak of 1419 cm^{-1} 1302 cm^{-1} is contributed by the stretching vibration of the C–N bond. The appearance of C-N bending vibrations was

determined at the peak of 992 cm^{-1}. Furthermore, the peak at 421 cm^{-1} corresponds to the Zn, Co-N stretch bond, which proves that the Zn^{2+} and Co^{2+} cations are linked to the nitrogen atom in methylimidazole to create Zn/Co-ZIF [14,15].

The BET results of Zn, Co, and ZIF are presented in Table 1. From here, the specific surface area of Zn/ Co- ZIF was 1311.4 m^2/g, and was higher than in the previous publication (225 m^2/g)[3]. Moreover, the material had a porous structure due to its high pore volume which contributed to activating PMS.

Table 1. Specific surface area and porosity of Zn/Co-ZIF

Sample	Specific surface area (m^2 g^{-1})	Pore volume (cm^3 g^{-1})	Pore size (nm)
Zn/Co - ZIF	1311.4	0.683	2.08

3.2. Effects of different parameters on MB degradation efficiency

Reaction conditions, including catalyst dose, PMS and MB concentration, and initial pH, were important for catalytic activity in practical applications. Influence of factors such as catalyst dose 0-80 mg/L, PMS concentration 0-1.22 mM, pH = 3.5–11 (Figure 3). The results of Figure 3a illustrates that, MB was decomposed with low efficiency (9.51%) by only PMS without catalyst. This due to the weak oxidation property of PMS (E^o=1.82V) compared to the free radicals SO$_4^{\bullet-}$, HO$^{\bullet}$, O$_2^{\bullet-}$, and ^{1}O$_2$ (E^o=2.2V-3.1V) [16]. However, MB decomposes quickly in the first 2.5 minutes with the presence of a catalyst, then a slight rise. MB decomposition efficiency advanced sharply with the catalyst, reaching 85.4–99.87%, approximating a catalyst concentration of 20 mg/L–80 mg/L. Established confirming degradation efficiency and financial choice, the optimal catalyst content was 40 mg/L. The effect of PMS concentration is shown in Figure 3b. MB decomposition efficiency was low (12.07%–61.41%) in the PMS range of 0.163–0.489 mM. The lack of PMS led to the limited formation of oxygen species. At PMS concentrations of 0.814–1.22 mM, MB decomposition efficiency reached 98%–99.57%. Therefore, a PMS concentration of 0.814 mM was chosen to investigate the catalytic activity.
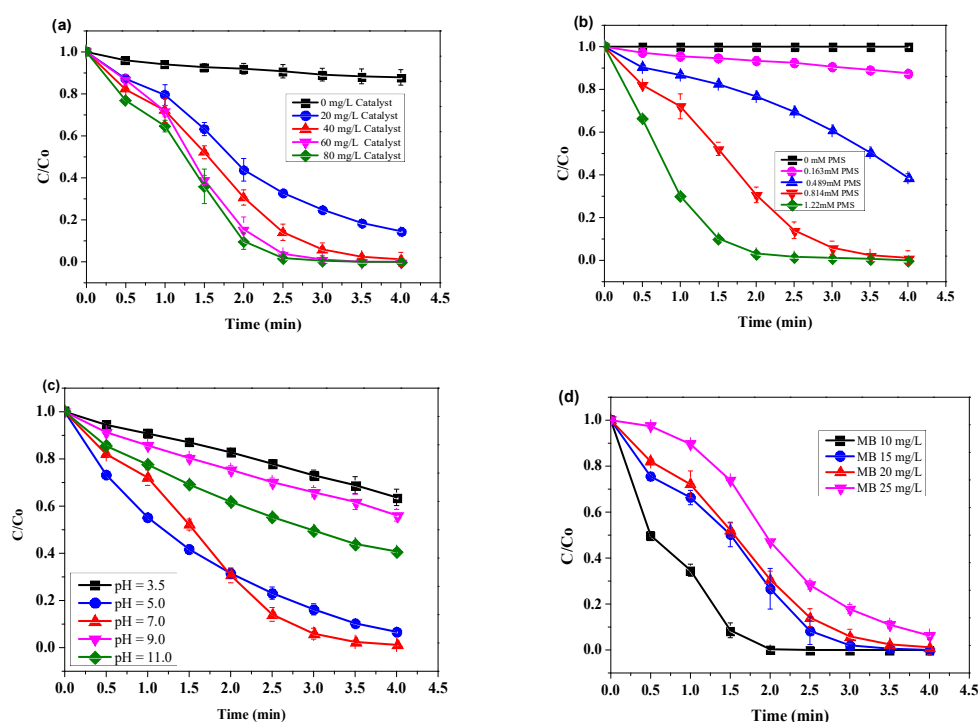
Fig 3: Effect of (a) catalyst dosage, (b) PMS concentration, (c) initial pH and (d) MB concentration on the degradation of MB in Zn/Co-ZIF/PMS system.

The effect of pH on MB degradation in the ZnCo-ZIF/PMS system is shown in Fig 3c. Remaining at pH 5 and 7 dissolved MB decomposition was 96.07% and, 98% respectively. At pH 11 the efficiency is 85.84%, however at pH 3.5 and 9, the efficiency dropped to 36.69% and 58.72%, respectively. In an acidic

environment, the quenching process of the free radicals $SO_4^{\bullet-}$ and $^\bullet OH$ occurs according to the reactions. In a strongly alkaline environment, the radical $SO_4^{\bullet-}$ was converted into $^\bullet OH$, reducing the oxidation properties of free origin[17]. In subsequent studies, pH = 7.0 was selected. At 40 mg/L Zn/Co-ZIF /0.814mM PMS system at pH=7.0, the MB decomposition efficiency decreased from 99.9% to 93.74% as the MB concentration went up from 10 mg/L to 25 mg/L (Fig 3d). The system quickly removed methylene blue (MB) within the 2 – 3 minutes, demonstrating its ability to degrade this substance. As a result, a MB concentration of 20 mg/L was chosen for the further experiment.

The decomposition properties of the Zn/Co-ZIF /PMS system for different dyes, including cationic (MB, RhB) and azo (MO, DB71, CR), were also tested to determine their applicability in complex real systems. Figure 4 demonstrates the degradation efficiency of various dyes in the Zn/Co-ZIF/PMS system within 4 min. All cationic and azo dyes could be effectively degraded (79.85%–98.22%) during short-time activation, demonstrating the extensive pertinence of the Zn/Co-ZIF/PMS system for many various organic wastewater treatment systems has practical purposes.
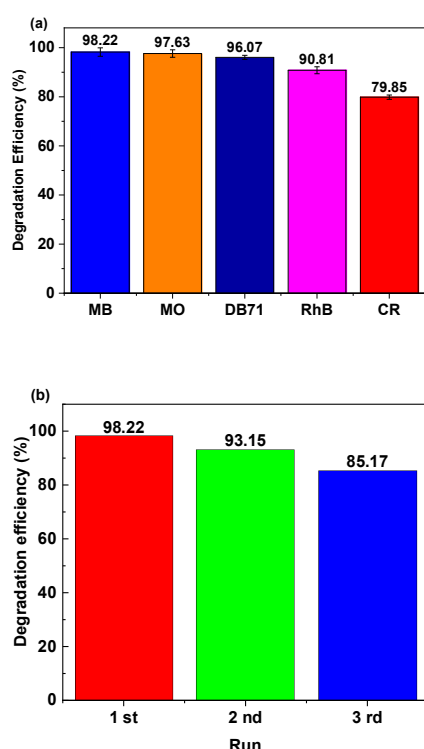
Fig 4: (a) The degradation efficiency of Zn/Co-ZIF/PMS for different dyes in 4 min (b) Three cycles of MB degradation by Zn/Co-ZIF activated PMS (catalyst dosage = 40 mg/L, PMS concentration = 0.814mM, dye concentration = 20 mg/L, pH=7.0, T = 25 °C)

The reusability of the Zn/Co-ZIF catalyst was evaluated through multiple reuse cycles. Zn/Co-ZIF material samples were collected by centrifugation, washed several times with double-distilled water and ethanol to remove decomposition products adsorbed on the surface, then dried at 80°C for 6 hours. The catalyst was then used for PMS activation to decompose MB under the same conditions. Results in Figure 4b show that after 3 reuse cycles, the MB decomposition efficiency decreased by 13.05%, indicating the potential application of the material in environmental treatment.

3.3. Determination of active species and activation mechanisms

The activation of PMS by Zn/Co-ZIF forms different active forms. To determine the contribution of active oxygen to MB decomposition, quenching experiments were conducted. In previous studies, it has been shown that TBA, EtOH, p-BQ, and FFA could selectively quench active oxygen species $HO^\bullet$, $SO_4^{\bullet-}$, $O_2^{\bullet-}$ and $^1O_2$ [11,17]. In this study, concentrations of TBA 500 mM, EtOH 500 mM, p-BQ 1 mM, and FFA 10 mM were used. Figure 5a shows that the MB removal efficiency was almost unchanged in the presence of 500 mM TBA, proving that $^\bullet OH$ had small role. The decomposition of MB was 50.01% when adding 500 mM EtOH, which shows that $SO_4^{\bullet-}$ radical plays an important role in removing pollutants. In addition, when adding 1 mM p-BQ, the MB treatment efficiency decreased sharply and reached 54.44%, claiming $O_2^{\bullet-}$ contributed to the reaction. However, the MB efficiency went down sharply at 10 mM FFA, to 18.58%, which means $^1O_2$ had significant attribute to system. Thus, the decomposition of MB had contributions from the active forms $SO_4^{\bullet-}$, $O_2^{\bullet-}$, and $^1O_2$. $^1O_2$ had a decisive role in removing MB. This can be explained by free radicals such as $HO^\bullet$, $SO_4^{\bullet-}$ and $O_2^{\bullet-}$ acting as precursors to form $^1O_2$, which was also consistent with previous studies [18,19]. The proposed activation reaction mechanism of the Zn/Co-ZIF/PMS system (Figure 5b) was related to the effective redox cycle of Co^{2+} and Co^{3+} (reactions 1-3) [4, 17]. In the research of Wu and coworker, the XPS proved the existence of Zn 2p peak (+2) and Co 2p peak (+2) [20]. The Co 2p1/2 spectral peak dropped to 778.46 eV, showing that the reduction process caused a change into a metallic state [21]. Research of Chen et al., proved the valence state of Co by XPS spectrum, assigned for N-coordinated Co^{3+}/Co^{2+} (Co-N) at 779.8 (Co^{3+}) and 781.6 eV (Co^{2+}) [22]. Moreover, Lei et al., confirmed that Co^{2+} and Co^{3+} implicated in PMS activation (Zn/Co-ZIF) with the decrease of Co^{2+} by 7.7% [23]. The formation of active oxygen species such as $HO^\bullet$, $SO_4^{\bullet-}$, $O_2^{\bullet-}$ and

$^1O_2$ can be explained by the reactions 4-9. Moreover, Zn/Co-ZIFs exhibited a substantial specific surface area and significant porosity, which promote pollutant adsorption and improve pollutant decomposition performance. Finally, reactive oxygen species attack MB forming intermediate degradation and mineralization products (reaction 10)

$$\equiv Co^{2+} + HSO_5^- \rightarrow\ \equiv Co^{3+} + SO_4^{\bullet -} + OH^- \quad (1)$$

$$\equiv Co^{2+} + 2HSO_5^- \rightarrow\ \equiv Co^{3+} + O_2^{\bullet -} + 2HSO_4^- \quad (2)$$

$$\equiv Co^{3+} + HSO_5^- \rightarrow\ \equiv Co^{2+} + SO_5^{\bullet -} + H^+ \quad (3)$$

$$SO_4^{\bullet -} + H_2O \rightarrow HO^\bullet + HSO_4^- \quad (4)$$

$$4SO_4^{\bullet -} + 2H_2O \rightarrow 4HSO_4^- + 1O_2 \quad (5)$$

$$2SO_5^{\bullet -} + H_2O \rightarrow 2HSO_4^- + 1.5^1O_2 \quad (6)$$

$$HO^\bullet + O_2^{\bullet -} \rightarrow 1O_2 + HO^- \quad (7)$$

$$HSO_5^- \rightarrow SO_5^{2-} + H^+ \quad (8)$$

$$SO_5^{2-} + HSO_5^- \rightarrow 1O_2 + 2SO_4^- + H^+ \quad (9)$$

$$^1O_2, SO_4^{\bullet -,} O_2^{\bullet -} + MB \rightarrow CO_2 + H_2O + NO_3^- + \text{degradation products} \quad (10)$$
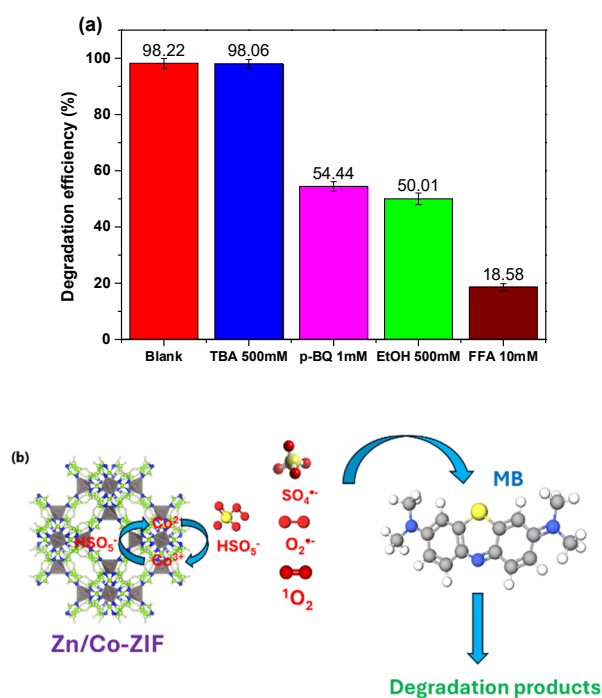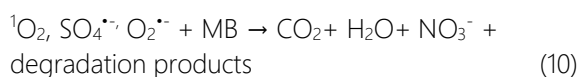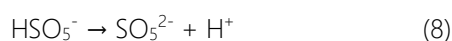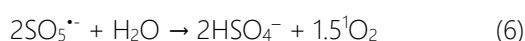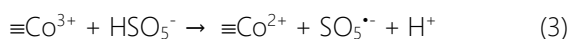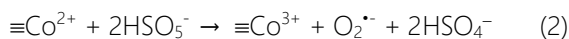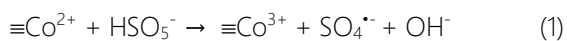
Fig 5: (a) Effect of radical scavengers on MB degradation, (b) proposed activation mechanism of Zn/Co-ZIF/PMS for MB degradation.

4. Conclusion

In this study, bimetallic metal Zn/Co-ZIF was easily synthesized by the solvothermal method at room temperature. Characterization was analyzed using techniques such as SEM, EDX, XRD, FT-IR, and BET. The results indicated that Zn/Co-ZIF had a porous structure with a large surface area and could activate PMS to oxidize various organic dyes, including congo red, directly blue 71, methyl orange, rhodamine B, and methylene blue with high efficiency (79.85%–98.22%). The optimal conditions are as follows: catalyst dosage was 40 mg/L, PMS dosage was 0.814 mM, initial pH was 7.0, MB concentration was 20 mg/L, and MB degradation reached 98.22 % within 4 minutes. In addition, the quenching tests indicated that $SO_4^{\bullet -}$, $O_2^{\bullet -}$ and $^1O_2$ were the main active species participating in the MB decomposition reaction. After 3 recycles, the removal efficiency of MB slightly decreased with 85.13%.

Acknowledgments

References

1. Y. Lai, Z. Sun, H. Wen, H. Ding, Colloids and Surfaces A: Physicochemical and Engineering Aspects 689 (2024) 133694. https://doi.org/10.1016/j.colsurfa.2024.133694
2. W. Zhao, Q. Shen, T. Nan, M. Zhou, Y. Xia, G. Hu, Q. Zheng, Y. Wu, T. Bian, T. Wei, C. Zhang, Journal of Alloys and Compounds 958 (2023) 170370. https://doi.org/10.1016/j.jallcom.2023.170370
3. F. Ling, X. Xiao, Y. Li, W. Li, New Journal of Chemistry 46 (2022) 18917. 10.1039/D2NJ02846H
4. Z. Wu, Y. Wang, Z. Xiong, Z. Ao, S. Pu, G. Yao, B. Lai, Applied Catalysis B: Environmental 277 (2020) 119136. https://doi.org/10.1016/j.apcatb.2020.119136
5. K.-Y.A. Lin, H.-A. Chang, Journal of the Taiwan Institute of Chemical Engineers 53 (2015) 40. https://doi.org/10.1016/j.jtice.2015.02.027
6. B. Yao, S.-K. Lua, H.-S. Lim, Q. Zhang, X. Cui, T.J. White, V.P. Ting, Z. Dong, Microporous and Mesoporous Materials 314 (2021) 110777. https://doi.org/10.1016/j.micromeso.2020.110777
7. M. Pu, D. Ye, J. Wan, B. Xu, W. Sun, W. Li, Separation and Purification Technology 299 (2022) 121716. https://doi.org/10.1016/j.seppur.2022.121716
8. M. Taheri, T.G. Enge, T. Tsuzuki, Materials Today Chemistry 16 (2020). https://doi.org/10.1016/j.mtchem.2019.100231
9. H.T.T. Nguyen, H.G. Dang, H.V.T. Luong, L.N.H. Cao, T.N.M. Ngo, T.B.N. Pham, T.T. Nguyen, Q.C.T. Nguyen, M.N.J.R.K. Nguyen, Mechanisms, Catalysis, 135 (2022) 2099. https://doi.org/10.1007/s11144-022-02240-8
10. J. Zhang, X. Yan, X. Hu, R. Feng, M. Zhou, Chemical Engineering Journal 347 (2018) 640. https://doi.org/10.1016/j.cej.2018.04.132

11. N.T. Dung, D.T.H. Ha, V.D. Thao, N.P. Thao, T.D. Lam, P.T. Lan, T.T. Trang, L.V. Ngan, B.D. Nhi, N.T. Thuy, K.-Y.A. Lin, N.N. Huy, Environmental Science and Pollution Research (2024). https://doi.org/10.1007/s11356-024-32776-2

12. J. Zhao, Z. Li, S. Yao, C. Hu, J. Wang, X. Feng, Journal of Materials Science: Materials in Electronics 31 (2020) 13889.https://doi.org/10.1007/s10854-020-03948-w

13. M. Loloei, S. Kaliaguine, D. Rodrigue, Separation and Purification Technology 296 (2022) 121391. https://doi.org/10.1016/j.seppur.2022.121391

14. N.T. Dung, L.M. Thu, U.T.D. Thuy, V.T. Thien, N.T. Thuy, N.T.C. Tien, K.-Y.A. Lin, N.N. Huy, Environmental Science: Nano 9 (2022) 3973. https://doi.org/10.1039/D2EN00219A

15. P. Utpalla, J. Mor, J. Bahadur, S.K. Sharma, Journal of Solid State Chemistry 316 (2022) 123601. https://doi.org/10.1016/j.jssc.2022.123601

16. C. Liang, S. Yin, P. Huang, S. Yang, Z. Wang, S. Zheng, C. Li, Z. Sun, Chemical Engineering Journal 482 (2024) 148969. https://doi.org/10.1016/j.cej.2024.148969

17. N.Q. Tung, D.T.C. Van, D.X. Thang, N.T.K. An, T.T. Trang, B.D. Nhi, N.P. Thao, L.T. Son, N.N. Huy, N.T. Dung, Journal of Environmental Chemical Engineering 11 (2023) 110127. https://doi.org/10.1016/j.jece.2023.110127

18. M. Wang, F. Wang, P. Wang, H. Chu, H. Fu, C. Zhao, C.-C. Wang, Y. Zhao, Separation and Purification Technology 326 (2023) 124806. https://doi.org/10.1016/j.seppur.2023.124806

19. Y. Long, S. Li, P. Yang, X. Chen, W. Liu, X. Zhan, C. Xue, D. Liu, W. Huang, Separation and Purification Technology 286 (2022) 120470. https://doi.org/10.1016/j.seppur.2022.120470

20. Z. Wu, Y. Wang, Z. Xiong, Z. Ao, S. Pu, G. Yao, B. Lai, Applied Catalysis B: Environmental 277 (2020). https://doi.org/10.1016/j.apcatb.2020.119136

21. M. Cheng, Y. Huo, Z. Diao, G. Song, D. Chen, L. Hang, L. Kong, Separation and Purification Technology 327 (2023). https://doi.org/10.1016/j.seppur.2023.124976

22. Y. Chen, K. Cui, T. Liu, M. Cui, Y. Ding, Y. Chen, X. Chen, W.W. Li, C.X. Li, Sci Total Environ 850 (2022) 158055. https://doi.org/10.1016/j.scitotenv.2022.158055

23. Y. Lei, W. Sun, S.K. Tiwari, K. Thummavichai, O. Ola, X. Qin, Z. Ma, N. Wang, Y. Zhu, Journal of Environmental Chemical Engineering 9 (2021) 106885. https://doi.org/10.1016/j.jece.2021.106885